

ON THE NUMERICAL REQUIREMENTS OF RANS AND HYBRID TURBULENCE MODELS

Filipe S. Pereira^{*‡}, Guilherme Vaz[†] and Luís Eça[‡]

^{*}Maritime Research Institute Netherlands (MARIN) Academy
Research & Development Department
Wageningen, The Netherlands
e-mail: f.pereira@academy.marin.nl

[†] Maritime Research Institute Netherlands (MARIN)
Research & Development Department
Wageningen, The Netherlands
e-mail: g.vaz@marin.nl

[‡] Instituto Superior Técnico (IST), Universidade Técnica de Lisboa (UTL)
Mechanical Engineering Department
Lisbon, Portugal
e-mail: luis.eca@tecnico.ulisboa.pt

Key words: Numerical Uncertainty, Numerical Errors, Turbulence Modelling, Circular Cylinder, RANS, Hybrid Models

Abstract. The evaluation of different mathematical models for the prediction of turbulent flows depends on the ability to reduce the numerical error to negligible levels, i.e. to values clearly below the modelling error. In this work we assess the numerical requirements, i.e. grid/time refinement, iterative and statistical convergence levels, to achieve such goal for three different mathematical models: Reynolds-Averaged Navier-Stokes (RANS) equations supplemented by an eddy-viscosity model; Delayed Detached Eddy Simulation (DDES) and eXtra Large Eddy Simulation (XLES). To this end, numerical simulations are performed with RANS and the two hybrid models (blend of RANS and LES) for the flow around a circular cylinder at a Reynolds number of 3900. The results show that the grid/time refinement and iterative and statistical (for DDES and XLES) convergence levels required to achieve such goal are clearly more demanding than those usually found in the open literature, especially for the two models that simulate directly the large scales of turbulence, DDES and XLES. Nonetheless, the comparison of mean flow quantities with available experimental data suggests that the hybrid models reduce the modelling error when compared to RANS.

1 INTRODUCTION

The role of Computational Fluid Dynamics (CFD) has increased over the last decades, and currently is an important tool on the marine engineering design process. Most engineering interest applications deal with turbulent flows, characterized by a wide range of turbulent scales. This feature makes their prediction by directly solving the Navier-Stokes equations not feasible for engineering applications due to the temporal and spatial grid requirements (time step and cell size) to capture all turbulent scales. As a result, turbulence modelling is necessary. However, the development of mathematical models capable of combining accuracy with reasonable time steps and cells sizes is a difficult task, making turbulence modelling one of the major challenges of fluid dynamics, and CFD.

Hybrid mathematical models have been developed to fulfil the gap between Reynolds-Averaged Navier-Stokes (RANS) equations and Large-Eddy Simulations (LES) models. RANS models tend to poorly predict flows with massive separation. On the other hand, LES is still too demanding for common engineering applications, in particular for wall-bounded flows. Therefore, the majority of these hybrid models combines RANS models in boundary layers with LES models (or LES based) in detached regions. As a result, the computational demands are substantially reduced, while it can be expected that the modelling accuracy improves when compared to RANS models. Nevertheless, the numerical requirements are still much larger than for RANS models, especially due to the different meaning of the dependent variables in the "LES region" of the flow, which are no longer mean quantities but instantaneous values that require statistical convergence to obtain reliable mean flow predictions. Hybrid mathematical models are a class of Scale-Resolving Simulation (SRS) models due to their ability to resolve part of the turbulence field. Therefore, for the sake of simplicity, these models are called SRS models in this paper. Scale-Adaptive Simulation (SAS) [1], Detached-Eddy Simulation (DES) [2], and eXtra Large-Eddy Simulation (XLES) [3] are examples of such modelling approaches.

This paper addresses the numerical requirements, i.e. grid/time refinement, iterative and statistical convergence levels, to obtain numerical uncertainties that allow a reliable comparison between three mathematical models for the prediction of turbulent flows: RANS, Delayed DES (DDES) and XLES. To this end, the flow over a circular cylinder is simulated at a Reynolds number of 3900. This test-case exhibits complex turbulent and laminar phenomena, and so it is a challenging test case. All the numerical simulations are executed with ReFRESHO viscous-flow CFD code [4]. The paper is structured as follows. Section 2 presents a brief description of the turbulence models studied in this paper, while section 3 introduces the numerical simulations details: ReFRESHO solver, case study including domain size and boundary conditions, and numerical settings; the numerical results are discussed in section 4, and section 5 summarizes the conclusions and presents the future work.

2 TURBULENCE MODELLING

In most engineering applications a statistical or filtered approach is applied for the solution of the Navier-Stokes equations (NSE). Depending on the type of statistical approach, different mathematical/turbulence models are derived, such as RANS or LES. Herein, we define a general filtering approach (a panoply of spatial and temporal filters is available in the literature), which decomposes a general quantity Φ as,

$$\Phi = \langle \Phi \rangle + \phi, \quad (1)$$

where $\langle \Phi \rangle$ is the resolved part of the Φ field, and ϕ is the unresolved or modelled component. For RANS models, the complete turbulent field is modelled, and so $\langle \Phi \rangle$ represents just the mean flow field (ensemble averaging) and ϕ the turbulent field. On the other hand, for SRS models $\langle \Phi \rangle$ stands for the resolved part of the instantaneous field while ϕ is the modelled part of the turbulent field. Applying this general filtering approach to the NSE, and assuming an incompressible and Newtonian fluid, leads to,

$$\frac{\partial \langle V_i \rangle}{\partial t} + \frac{\partial \langle V_i \rangle \langle V_j \rangle}{\partial x_j} = -\frac{1}{\rho} \frac{\partial \langle P \rangle}{\partial x_i} + \frac{\partial}{\partial x_j} \left[\nu \frac{\partial \langle V_i \rangle}{\partial x_j} \right] + \frac{\partial \tau(v_i, v_j)}{\partial x_j}, \quad (2)$$

$$\frac{\partial \langle V_i \rangle}{\partial x_j} = 0, \quad (3)$$

where V stands for the velocity, P for the relative pressure, and ν for the kinematic viscosity. Moreover, depending on the turbulence model, τ represents the Reynolds or sub-grid stresses (for RANS and SRS models, respectively). Applying the Boussinesq hypothesis, τ is defined as,

$$\tau(v_i, v_j) = \nu_t \left(\frac{\partial \langle V_i \rangle}{\partial x_j} + \frac{\partial \langle V_j \rangle}{\partial x_i} \right) - \frac{2}{3} \delta_{ij} k. \quad (4)$$

In equation 4, k is the unresolved component of the total turbulence kinetic energy, K , and ν_t an eddy-viscosity which models the effect of the unresolved turbulent field on the resolved field, $\langle \Phi \rangle$. These variables are extra unknowns, and so it is required a closure model (also named turbulence model) for RANS and SRS models to close the system of equations. Several methodologies are available for RANS and SRS models. Those used in this work are presented in sections 2.1 to 2.3. Note, however, that all turbulent quantities computed within these closure models are modelled or unresolved quantities.

2.1 Reynolds-Averaged Navier-Stokes Equations

The two-equation $k - \omega$ SST model [5] blends the standard $k - \epsilon$ and $k - \omega$ models to combine their main advantages, and it is able to account the effect of the principal turbulent shear-stresses. It calculates the eddy-viscosity, ν_t , from,

$$\nu_t = \frac{a_1 k}{\max \{a_1 \omega, \langle S \rangle F_2\}}, \quad (5)$$

using two transport equations to determine k and ω ,

$$\frac{\partial k}{\partial t} + \frac{\partial k \langle V_j \rangle}{\partial x_j} = P_k - \beta^* k \omega + \frac{\partial}{\partial x_j} \left[(\nu + \nu_t \sigma_k) \frac{\partial k}{\partial x_j} \right], \quad (6)$$

$$\frac{\partial \omega}{\partial t} + \frac{\partial \omega \langle V_j \rangle}{\partial x_j} = \frac{\alpha}{\nu_t} P_k - \beta \omega^2 + \frac{\partial}{\partial x_j} \left[(\nu + \nu_t \sigma_\omega) \frac{\partial \omega}{\partial x_j} \right] + \frac{2\sigma_{\omega^2}}{\omega} (1 - F_1) \frac{\partial \omega}{\partial x_j} \frac{\partial k}{\partial x_j}. \quad (7)$$

In equations 5 to 7, $\langle S \rangle$ is the invariant measure of the strain-rate tensor (computed from the resolved velocity, $\langle V \rangle$), while P_k is the production of (modelled) turbulence kinetic energy. Moreover, a_1 , β^* , σ_k , α , β , σ_ω , σ_{ω^2} , F_1 , and F_2 are constants and blending functions given in [5].

2.2 Delayed Detached-Eddy Simulation

Delayed Detached-Eddy Simulation (DDES) [6] is a mathematical model that combines RANS in boundary layers, with a LES based model in outer and detached turbulent flow regions. The version used in the present work relies on the RANS model described in section 2.1, [5]. The dissipation term of the k transport equation is modified to rely on the turbulent length scale, l_t ,

$$\frac{\partial k}{\partial t} + \frac{\partial k \langle V_j \rangle}{\partial x_j} = P_k - \frac{k^{3/2}}{l_t} + \frac{\partial}{\partial x_j} \left[(\nu + \nu_t \sigma_k) \frac{\partial k}{\partial x_j} \right], \quad (8)$$

defined as,

$$l_t = l_{RANS} - f_d \max(l_{RANS} - l_{LES}, 0). \quad (9)$$

In equation 9, l_{RANS} stands for the RANS length scale (integral length scale when in RANS mode), $l_{RANS} = \sqrt{k}/(\beta\omega)$, and l_{LES} for the LES length scale, $l_{LES} = C_{DES}\Delta$ (Δ is the maximum cell length). Furthermore, f_d is the empirical delay function that is defined in [6].

2.3 EXtra Large-Eddy Simulation

The eXtra Large-Eddy Simulation (XLES) [3] is a hybrid mathematical model based on the TNT version of the $k - \omega$ model. This formulation solves the following transport equations,

$$\frac{\partial k}{\partial t} + \frac{\partial k \langle V_j \rangle}{\partial x_j} = P_k - \beta^* \frac{k^{3/2}}{l_t} + \frac{\partial}{\partial x_j} \left[(\nu + \nu_t \sigma_k) \frac{\partial k}{\partial x_j} \right], \quad (10)$$

$$\frac{\partial \omega}{\partial t} + \frac{\partial \omega \langle V_j \rangle}{\partial x_j} = \frac{\alpha}{\nu_t} P_k - \beta \omega^2 + \frac{\partial}{\partial x_j} \left[(\nu + \nu_t \sigma_\omega) \frac{\partial \omega}{\partial x_j} \right] + \frac{\sigma_d}{\omega} \max \left\{ \frac{\partial k}{\partial x_i} \frac{\partial \omega}{\partial x_i}, 0 \right\}, \quad (11)$$

with the eddy-viscosity obtained from,

$$\nu_t = \min \left\{ \frac{k}{\omega}, l_t k^{1/2} \right\}. \quad (12)$$

l_t stands for a turbulent length scale that is defined as,

$$l_t = \min \left\{ \sqrt{k}/\omega, C_1 \Delta \right\}. \quad (13)$$

The constants β^* , σ_k , α , β , σ_ω , σ_d and C_1 are given in [3, 7].

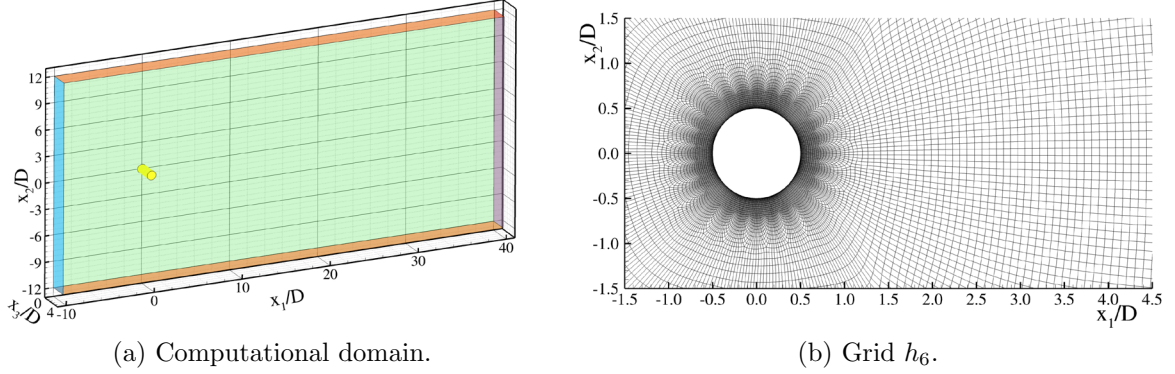
3 NUMERICAL SIMULATIONS DETAILS

3.1 ReFRESKO

ReFRESKO is a viscous-flow CFD code that solves multiphase (unsteady) incompressible flows using the Navier-Stokes equations, complemented with turbulence models, cavitation models and volume-fraction transport equations for different phases. The equations are discretised using a finite-volume approach with cell-centred collocated variables, in strong-conservation form, and a pressure-correction equation based on the SIMPLE algorithm is used to ensure mass conservation. Time integration is performed implicitly with first or second-order backward schemes. At each implicit time step, the non-linear system for velocity and pressure is linearised with Picard's method and either a segregated or coupled approach is used. A segregated approach is always adopted for the solution of all other transport equations. The implementation is face-based, which permits grids with elements consisting of an arbitrary number of faces (hexahedrals, tetrahedrals, prisms, pyramids, etc.), and if needed h-refinement (hanging nodes). State-of-the-art CFD features such as moving, sliding and deforming grids, as well automatic grid refinement are also available. For turbulence modelling, traditional one and two-equations RANS eddy-viscosity models are available, as well as the SRS models studied in the present work. The code is parallelised using MPI and subdomain decomposition, and runs on Linux workstations and HPC clusters. ReFRESKO is currently being developed and verified at MARIN (in the Netherlands) in collaboration with IST (in Portugal), USP-TPN (University of Sao Paulo, Brasil), TUDelft (Technical University of Delft, the Netherlands), UoS (University of Southampton, UK) and recently UTwente (University of Twente, the Netherlands) and Chalmers (Chalmers University, Sweden) [4].

3.2 Case study

The selected test case is the flow around a circular cylinder at a Reynolds number of 3900 based on the undisturbed flow velocity, V_∞ , and cylinder diameter, D . The computational domain is defined in order to avoid disturbances from boundaries. The inlet and outlet boundaries are $x_1 = \text{const.}$ planes (x_1 is aligned with the incoming flow) located 10D upstream and 40D downstream of the cylinder centre, respectively. The top and bottom boundaries are $x_2 = \text{const.}$ planes (x_2 designates the transversal direction) 12D away from the cylinder centre. In the span-wise direction x_3 , the width of the domain is 3D and the lateral boundaries are $x_3 = \text{const.}$ planes. A scheme of the computational domain is depicted in figure 1a. At the inlet, we impose undisturbed velocity, k and ω , whereas the pressure is extrapolated from the interior of the domain. The turbulent variables values result from setting the turbulence intensity $I = 0.2\%$ and the ratio between turbulent and molecular viscosities $\mu_t/\mu = 10^{-3}$. The pressure is imposed at the top and bottom boundaries, while at the outlet the stream-wise derivatives of all dependent variables are equal to 0. In [8], it has been shown that boundary conditions for the lateral boundaries of a domain of 3D width are troublesome to impose. Therefore, in the present exercise


 Figure 1: Computational domain and 2D coarsest grid, h_6 .

we selected the simplest choice of symmetry conditions. We are aware that such choice will affect the modelling error independently of the selected turbulence model. However, choosing a sufficient width of the domain to avoid the problem would make the exercise too expensive. This issue was addressed in [8].

3.3 Numerical settings

The numerical simulations are carried out using a segregated approach to solve the momentum, pressure (continuity), and turbulence quantities transport equations. All space and time discretization schemes are second-order accurate. The simulations run on double precision, and iterative convergence is controlled by the maximum normalized residual¹ of all transport equations solved, c_{it} . Three different levels of c_{it} were tested to evaluate the influence of this component of the iterative error: 10^{-3} , 10^{-5} and 10^{-7} . However, the main calculations have used $c_{it} = 10^{-5}$. In this work, we have performed grid/time refinement studies for two (2D) and three-dimensional (3D) domains. In the 2D case, we have a set of six grids (designated by h_i^{2D}) with a coarsest grid of 34,578 cells (h_6^{2D}) and a finest grid of 167,480 cells (h_1^{2D}) covering a grid refinement ratio ($h_i/h_1 = \sqrt{N_1/N_i}$) of 2.2. The coarsest grid of this set is illustrated in figure 1b. Four dimensionless time steps ($\Delta t V_\infty/D$) are tested ranging from 0.002 (Δt_1^{2D}) to 0.2 (Δt_4^{2D}), which corresponds to a time refinement ratio ($\Delta t_j^{2D}/\Delta t_1^{2D}$) of 10. The 3D grids (designated by h_i^{3D}) were obtained by extruding the three coarsest 2D grids in the span-wise direction keeping the refinement ratio of the 2D grids in the x_3 direction. This leads to grids with 10^6 (h_3^{3D}) to 3×10^6 cells (h_1^{3D}). In the coarsest grid, $x_1^+ < 4.6$, $x_2^+ < 0.8$ and $x_3^+ < 80$. To study the effect of the span-wise grid density, we have generated a grid equivalent to h_3^{3D} , but with half the grid nodes in the x_3 direction (0.5×10^6 cells, h_4^{3D}). The dimensionless time step (Δt_j^{3D}) is tuned to obtain a Courant number in the turbulent flow region close to 1 (the maximum Courant number is 3.2 for the laminar and 1.5 for the turbulent flow regions). For grid h_3^{3D} , we have also tested time steps equal to $0.5\Delta t_3^{3D}$, $2\Delta t_3^{3D}$, $4\Delta t_3^{3D}$ and $8\Delta t_3^{3D}$.

¹normalized residuals are equivalent to variables differences in a simple Jacobi iteration.

All calculations are initialized with velocity, pressure and turbulent fields obtained from an initial (unsteady) RANS simulation, and at least 400 non-dimensional time units are calculated.

4 NUMERICAL RESULTS

The assessment of the numerical requirements of the RANS and SRS models is based on 4 selected flow quantities: the Strouhal number St , the drag C_D and lift C_L coefficients, and the mean stream-wise velocity (obtained from time-averaging $\langle V_1 \rangle$) along the centre-line downstream of the cylinder, $\vec{x} \approx (0.5 - 10.0; 0.0; 1.5)$. Time-averaged (designated by an overbar) and root mean squared (designated by rms) quantities are computed with the data of, at least, 250 dimensionless time units that cover more than 50 shedding cycles.

4.1 Numerical requirements

4.1.1 Two-dimensional grid and time-step refinement studies

An initial 2D grid/time refinement study including 24 calculations (6 grids and 4 time steps) was performed in order to estimate the grid and time refinement required to fulfil our goal: numerical uncertainties that allow a reliable evaluation of modelling errors. All simulations are carried out with $c_{it} = 10^{-7}$, and the procedure used to estimate the order of grid and time convergence and the numerical uncertainty is a generalized version of the procedure presented in [9]. The results obtained for the time-averaged drag coefficient, \overline{C}_D , root-mean-square lift coefficient, $(C_L)_{rms}$, and Strouhal number, St , are depicted in figure 2. The results show that for the present level of grid/time refinement the discretization error is mainly determined by the space discretization. The estimated numerical uncertainty is 6.9% for \overline{C}_D , 5.1% for $(C_L)_{rms}$ and 24.9% for St . These estimated numerical uncertainties demonstrate that the present level of grid refinement is too coarse to obtain negligible levels of numerical uncertainty with 2D RANS. This is a worrying result, because the level of grid refinement used in the 3D simulations (to be affordable) is coarser than in the 2D case.

4.1.2 Iterative convergence criterion at each time step

The three levels of c_{it} mentioned above (10^{-3} , 10^{-5} and 10^{-7}) were tested for RANS (2D and 3D²) and DDES. It is important to recall that c_{it} stands for the maximum normalized residual of all transport equations solved at a given time step. Figure 3 presents the time history of C_D obtained in grids h_6^{2D} and h_3^{3D} . It is clear that the smallest dependence of C_D on c_{it} is obtained for RANS 2D and the largest for DDES. In order to give a quantitative idea of this dependence, table 1 presents the values of \overline{C}_D and $(C_L)_{rms}$ for the three values of c_{it} tested. Table 1 also contains the maximum number of iterations

²The statistics of RANS predictions using $c_{it} = 10^{-7}$ are computed with less 20 shedding cycles than those with $c_{it} = 10^{-3}$ or $c_{it} = 10^{-5}$.

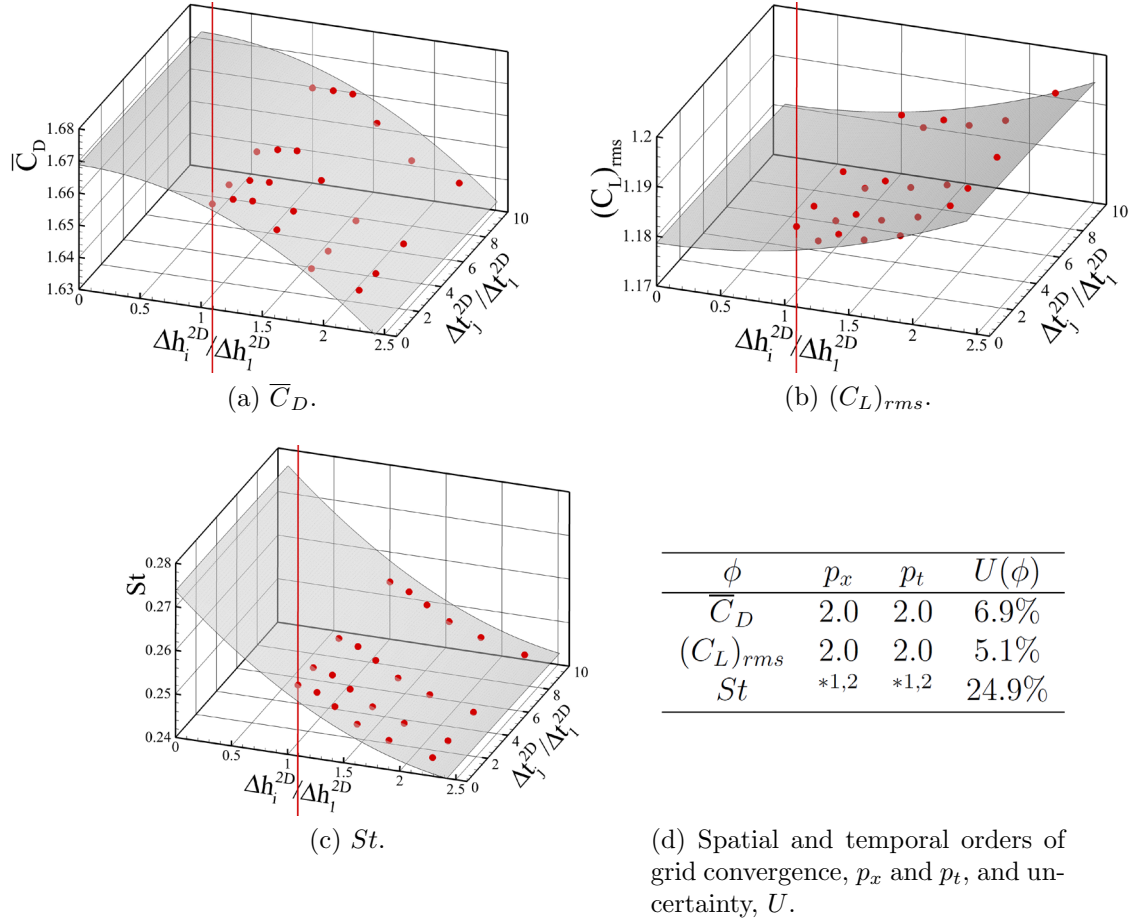


Figure 2: Time-averaged drag coefficient, \overline{C}_D , root-mean-square lift coefficient, $(C_L)_{rms}$, and Strouhal number, St , convergence with spatial ($1 \leq i \leq 6$) and temporal ($1 \leq j \leq 4$) resolution.*^{1,2} fit is made using first and second order exponent.

performed in each time step N_{iter} . Figure 4 illustrates $\langle \overline{V}_1 \rangle / V_\infty$ along the centreline downstream of the cylinder. For these flow conditions, grid density/time step and levels of c_{it} , there is a negligible influence of the iterative error at each time step for RANS 2D. For RANS 3D, the influence is mainly visible on $(C_L)_{rms}$ that reaches 4.5% difference between the solutions obtained with $c_{it} = 10^{-5}$ and $c_{it} = 10^{-7}$. On the other hand, DDES exhibits a significant influence of c_{it} for all selected variables (the differences on $(C_L)_{rms}$ between $c_{it} = 10^{-5}$ and $c_{it} = 10^{-7}$ raise to 10%). Bearing in mind that DDES tries to simulate part of turbulent (fluctuating) field, this is not a surprising result. Naturally, N_{iter} increases with the reduction of c_{it} for all the models tested. However, the largest increase is obtained for DDES that is the model that requires the smallest values of c_{it} .

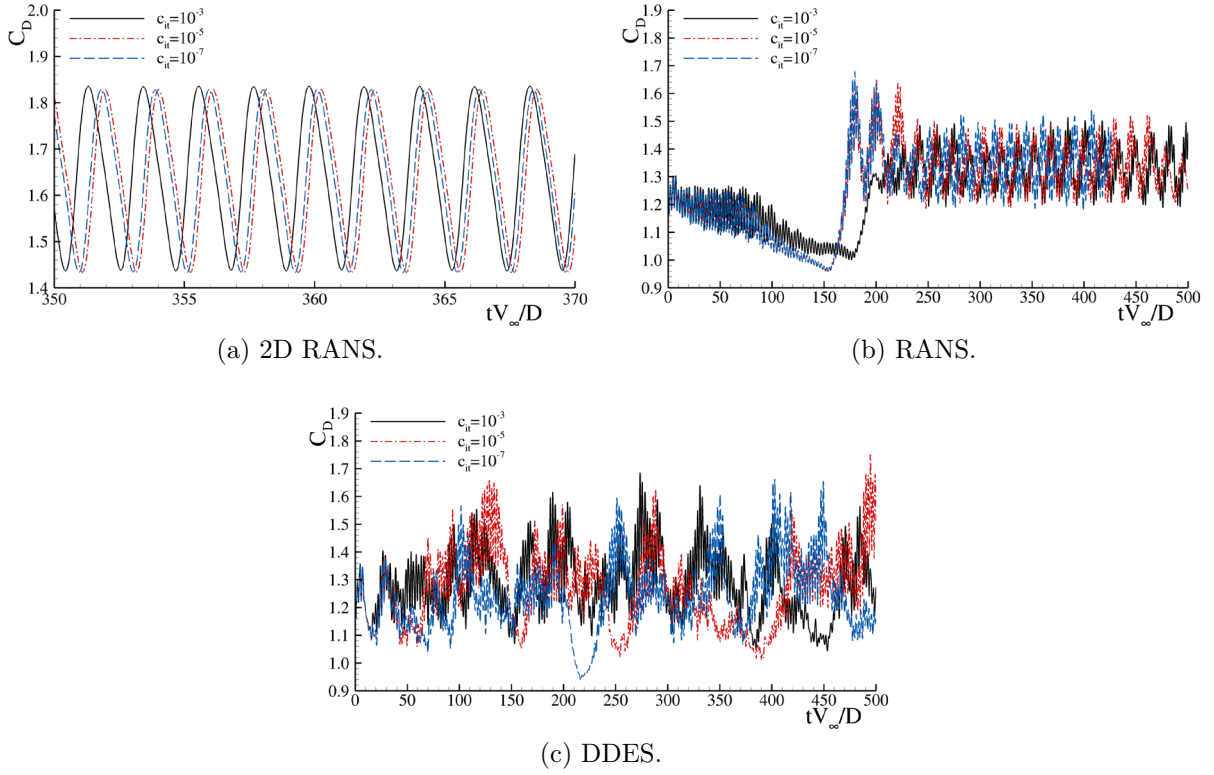


Figure 3: Time history of the drag coefficient, C_D , as a function of iterative convergence criterion, c_{it} . Results for 2D RANS ($h_6^{2D}, \Delta t_2^{2D}$), RANS and DDES ($h_3^{3D}, \Delta t_3^{3D}$).

Table 1: Time-averaged drag coefficient, \overline{C}_D , root-mean-square lift coefficient, $(C_L)_{rms}$, and maximum number of iterations, N_{iter} , as a function of iterative convergence criterion, c_{it} . Results for 2D RANS ($h_6^{2D}, \Delta t_2^{2D}$), RANS and DDES ($h_3^{3D}, \Delta t_3^{3D}$).

c_{it}	2D RANS			RANS			DDES		
	\overline{C}_D	$(C_L)_{rms}$	N_{iter}	\overline{C}_D	$(C_L)_{rms}$	N_{iter}	\overline{C}_D	$(C_L)_{rms}$	N_{iter}
10^{-3}	1.643	1.202	6	1.334	0.747	8	1.290	0.655	13
10^{-5}	1.638	1.192	27	1.335	0.750	28	1.279	0.645	37
10^{-7}	1.638	1.192	56	1.345	0.785	55	1.244	0.582	65

4.1.3 Simulation time

The iterative error in the calculation of unsteady flows does not depend only on the criteria applied at each time step. In general, the initial flow field does not correspond to an accurate solution of the selected mathematical model. Therefore, the simulation time

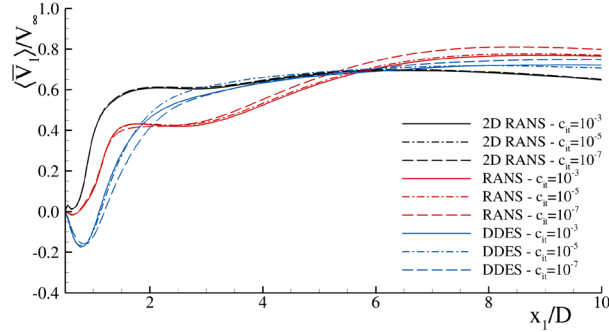


Figure 4: Time-averaged stream-wise velocity, $\langle \bar{V}_1 \rangle / V_\infty$, profile along the centreline downstream of the cylinder as a function of iterative convergence criterion, c_{it} . Results for 2D RANS (h_6^{2D} , Δt_2^{2D}), RANS and DDES (h_3^{3D} , Δt_3^{3D}).

must be sufficiently long to eliminate the influence of the initial conditions. Furthermore, the analysis of the flow field requires the use of statistics (even for RANS) and so the simulated interval must be long enough to obtain reliable (converged) results.

Figure 5a presents the time history of C_D obtained with RANS (2D and 3D), DDES and XLES in grids h_5^{2D} and h_2^{3D} . It is clear that RANS 2D exhibits the shortest influence of the initial condition (only about 30 dimensionless time units), whereas RANS 3D requires a simulation time almost 10 times larger than RANS 2D to eliminate the influence of the initial condition. Naturally, for DDES and XLES it is impossible to make such judgement from the data plotted in figure 5a.

The time-averaged values of C_D are depicted in figure 5b as a function of the time interval selected for its calculation $\Delta T^* = t_{final} - t$, which is one of the flow quantities that should require a smallest simulated time. The number of cycles required to obtain a converged estimate of \bar{C}_D is significantly smaller in RANS 2D than in RANS 3D, which is a natural consequence of the number of frequencies included in both time histories. On the other hand, the results obtained for DDES and XLES suggest that the simulated time is still not enough to obtain \bar{C}_D with a similar accuracy to that achieved in the RANS simulations.

A more reliable check of the statistical convergence of the mean value of the selected flow quantities may be performed with the auto-covariance method proposed in [10]³ that estimates the uncertainty of the mean value of a time series as a function of ΔT^* . According to [10], for sufficiently long time intervals the uncertainty of the mean value should decrease with $(\Delta T^*)^{-1}$. Figure 6 plots the uncertainty of \bar{C}_D , \bar{C}_L and $\langle \bar{V}_1 \rangle$ at $\vec{x} \approx (3.0; 0.0; 1.5)$ as a function of the simulated time for RANS, DDES and XLES in grids h_5^{2D} and h_2^{3D} . After an initial period, the uncertainty of the mean value starts to decrease with $(\Delta T^*)^{-1}$. The exceptions are the $U(\bar{C}_D)$ obtained with the DDES and XLES that

³Although initially developed for stationary processes, the method is also valid for statistically unsteady processes [11].

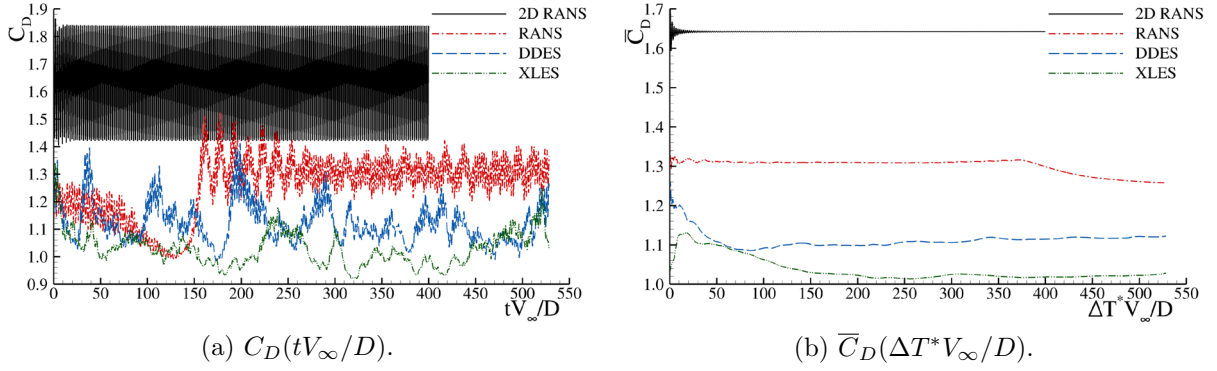


Figure 5: Time history of drag coefficient, C_D , and time-averaged drag coefficient, \overline{C}_D , obtained with 2D RANS ($h_5^{2D}, \Delta t_2^{2D}$), RANS, DDES and XLES ($h_2^{3D}, \Delta t_2^{3D}$).

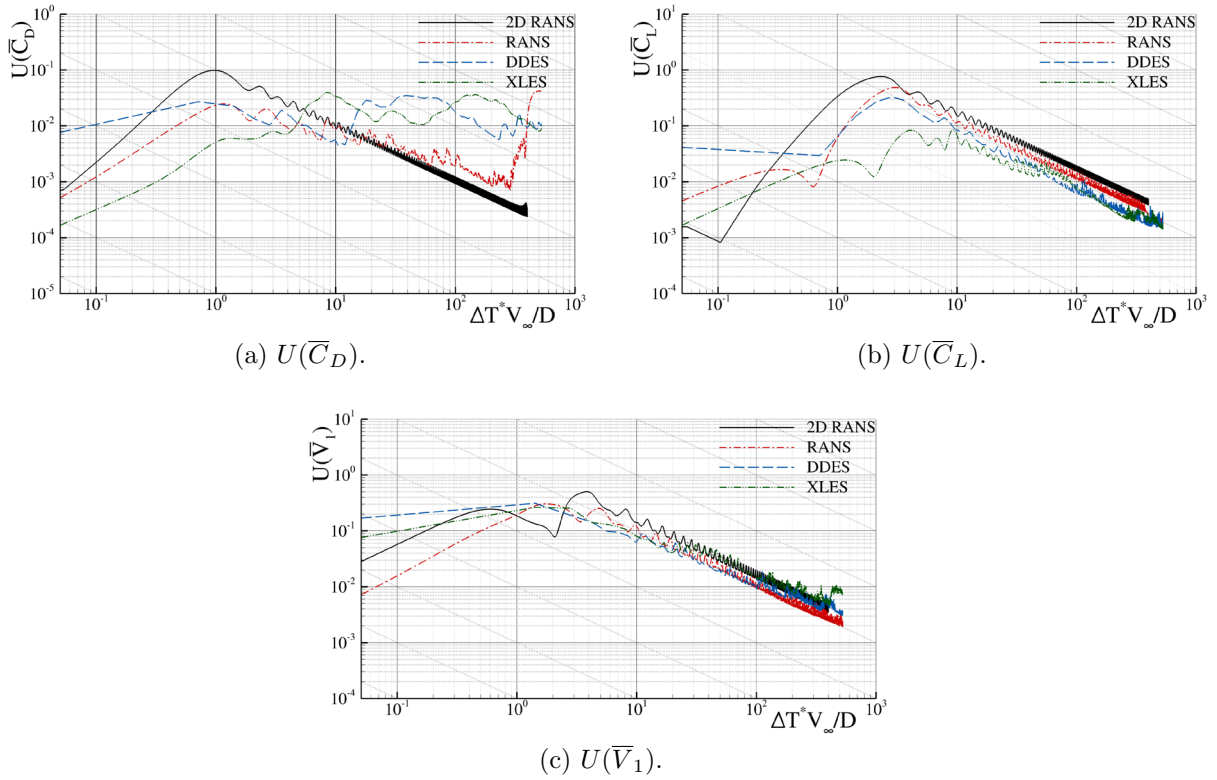


Figure 6: Auto-covariance method applied to time-averaged drag coefficient, \overline{C}_D , lift coefficient, \overline{C}_L , and resolved stream-wise velocity, $\langle \overline{V}_1 \rangle$, at $\vec{x} \approx (3.0; 0.0; 1.5)$. Results for RANS, DDES and XLES with h_2^{3D} and Δt_2^{3D} (h_5^{2D} and Δt_2^{2D} for 2D RANS).

remain above 1% confirming the trends observed in figure 5b. This only occurs for this quantity and might be related with the model variation with time, *i.e.* the filter varies in time, or to an insufficient simulated time. The plots of figure 6 also show the effect of the initial flow field in the simulation that leads to an increase of the uncertainty of the average quantities when the initial transient is included in the averaging process.

4.1.4 Spatial/temporal resolution

The influence of the spatial resolution on RANS, DDES and XLES was investigated with four grids, h_1^{3D} to h_4^{3D} , keeping constant the Courant numbers. Note, however, that these exercises include changes in the modelling and discretization errors when SRS models are used since their filter, l_t , is grid dependent. Figure 7 and table 2 present the results obtained with RANS, DDES and XLES for $\langle \bar{V}_1 \rangle / V_\infty$ along the centreline downstream of the cylinder, \bar{C}_D , $(C_L)_{rms}$, and St . The convergence of the RANS solutions is not monotonic and the differences between the data are similar to those obtained in the 2D exercise for the equivalent level of grid refinement. On the other hand, the solution obtained in h_4^{3D} is significantly different due to the lack of resolution in the span-wise direction. SRS models exhibit a significant dependence on the spatial resolution, which

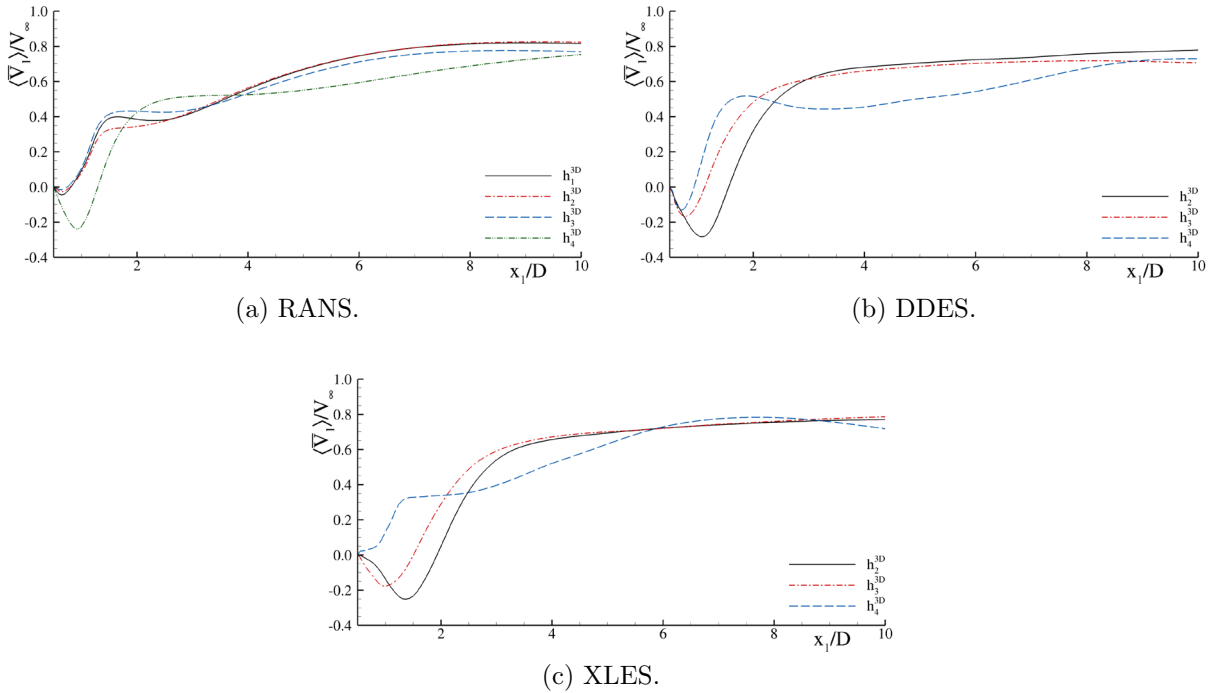


Figure 7: Time-averaged stream-wise velocity, $\langle \bar{V}_1 \rangle / V_\infty$, profile at the centreline as a function of spatial resolution, h_i^{3D} . Results for RANS, DDES and XLES.

Table 2: Time-averaged drag coefficient, \overline{C}_D , root-mean-square lift coefficient, $(C_L)_{rms}$, and Strouhal number, St , as a function of spatial resolution h_i^{3D} . Results for RANS, DES and XLES

h_i^{3D}	RANS			DDES			XLES		
	\overline{C}_D	$(C_L)_{rms}$	St	\overline{C}_D	$(C_L)_{rms}$	St	\overline{C}_D	$(C_L)_{rms}$	St
1	1.302	0.694	0.217	-	-	-	-	-	-
2	1.289	0.685	0.217	1.106	0.300	0.208	1.021	0.173	0.206
3	1.335	0.750	0.215	1.279	0.646	0.208	1.143	0.417	0.204
4	1.190	0.306	0.193	1.291	0.480	0.204	1.390	0.777	0.218

 Table 3: Time-averaged drag coefficient, \overline{C}_D , root-mean-square lift coefficient, $(C_L)_{rms}$, and Strouhal number, St , as a function of temporal resolution, $\Delta t^{3D} = \beta_j \Delta t_3^{3D}$. Results for RANS and DDES (h_3^{3D}).

β_j	RANS			DDES		
	\overline{C}_D	$(C_L)_{rms}$	St	\overline{C}_D	$(C_L)_{rms}$	St
1	1.339	0.757	0.215	1.245	0.579	0.208
2	1.335	0.745	0.215	1.279	0.646	0.208
3	1.335	0.758	0.215	1.263	0.605	0.208
4	1.323	0.728	0.215	1.273	0.623	0.204
5	1.338	0.778	0.215	1.318	0.701	0.211

is not a surprising result due to the explicit dependence of these models on the grid size. Naturally, the effect of the poor refinement in the span-wise direction is even stronger for the SRS models than for RANS. One of the main differences between RANS and SRS models is the meaning of the dependent variables that are average quantities for RANS and instantaneous values for SRS (in the “LES regions”). Therefore, a much stronger dependence of the results on the time step can be expected for SRS than for RANS. This is demonstrated in table 3 that presents the selected flow quantities obtained in grid h_3^{3D} with five different time steps using RANS and DDES.

4.2 Turbulence models comparison

Although we have not achieved our goal of negligible numerical uncertainties for the selected mathematical models, it is useful to compare the results obtained in the finest grids tested to evaluate the trends of the modelling error. Table 4 and figure 8 present the predicted \overline{C}_D , $(C_L)_{rms}$, St , and $\langle \overline{V}_1 \rangle / V_\infty$ along the centreline downstream of the cylinder.

Table 4: Time-averaged drag coefficient, \overline{C}_D , root-mean-square lift coefficient, $(C_L)_{rms}$, Strouhal number, St , minimum time-averaged stream-wise velocity, $(\langle \overline{V}_1 \rangle / V_\infty)_{min}$, at centreline, and time-averaged recirculation length, \overline{L}_r / D , as a function of turbulence model. Results for finest spatial and temporal resolution available.* approximate value.

Model	\overline{C}_D	$(C_L)_{rms}$	St	$ (\langle \overline{V}_1 \rangle / V_\infty)_{min} $	\overline{L}_r / D
RANS 2D	1.658	1.183	0.252	-	-
RANS	1.302	0.694	0.217	0.045	0.310
DDES	1.106	0.300	0.208	0.283	1.059
XLES	1.021	0.173	0.206	0.251	1.428
Experiments	1.00*[12]	0.05-0.10*[13]	0.208[14]	0.34[14]	1.51[14]

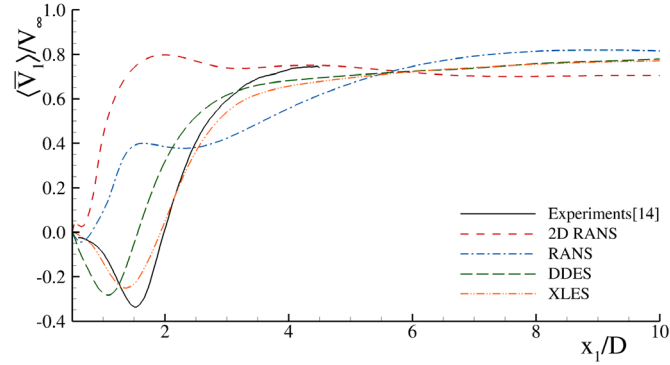


Figure 8: Time-averaged stream-wise velocity, $\langle \overline{V}_1 \rangle / V_\infty$, profile at the centreline as a function of turbulence model. Results for finest spatial and temporal resolution available.

The data suggest the following remarks:

- As already discussed in [8], assuming two-dimensional flow (RANS 2D) leads to a significant increase of the modelling error independently of the selected turbulence model;
- RANS calculations exhibit a difference to the experiments that is most likely larger than the numerical uncertainty, especially for $(C_L)_{rms}$. Note that the inexperienced user would select the RANS data from grid h_4^{3D} (see table 2) to obtain the best agreement to the experimental data. However, that would be a misleading result because it is just a consequence of the cancelling of model and numerical errors;
- The comparison of DDES and XLES with experiments shows a reduction of the comparison error, i.e. difference between simulations and experiments, suggesting that these models are reducing the modelling error. Therefore, the increase of

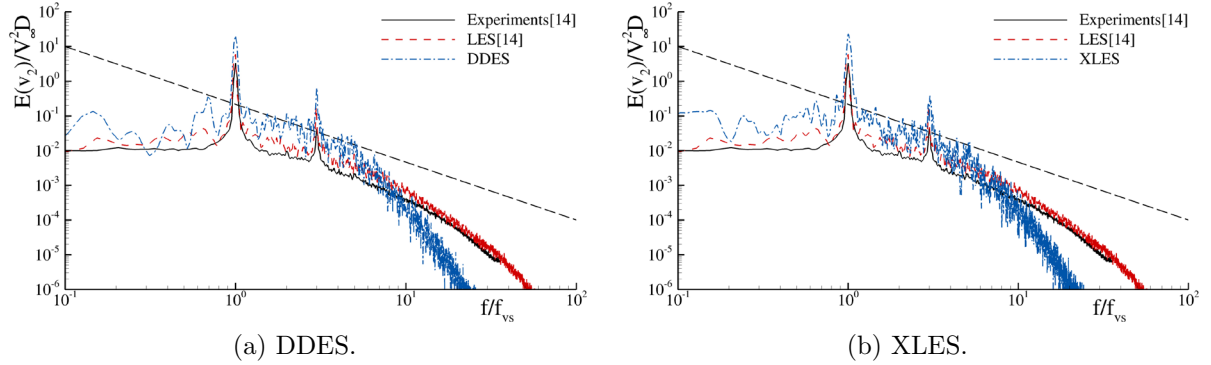


Figure 9: One-dimensional frequency energy spectrum at $\vec{x}/D \approx (3.0, 0.0, 1.5)$. The frequency is made dimensionless by the Strouhal frequency, f_{vs} . Results obtained with DDES and XLES for h_2^{3D} and Δt_2^{3D} .

computational resources required by the SRS models is most likely rewarded by an improvement in the modelling quality;

- The 1D energy spectrum of the cross-velocity at $\vec{x} \approx (3.0; 0.0; 1.5)$, figure 9, shows that at this location the solution entered into the inertial range. Although it is still far from reaching LES levels, when compared to RANS, these models show already a significant improvement in the prediction of the selected mean flow quantities.

5 CONCLUSIONS

This work investigates the role of the numerical requirements of distinct mathematical models for the prediction of turbulent flows. The selected models are RANS and two hybrid models: DDES and XLES. To this end, the flow past a circular cylinder at a Reynolds number of 3900 is analysed. The results obtained in the present study lead to the following conclusions:

- The grid/time refinement studies show that for the tested levels of grid/time refinement the discretization error is dominated by the spatial discretization. Naturally, such assessment is troublesome to make in SRS models due to the link of the mathematical model to the grid size and to the need to determine the instantaneous flow field;
- The influence of the iterative convergence criteria applied at each time step is stronger for the SRS models than for RANS. For the present level of grid/time refinement, it is obvious that the usual ”three-orders of magnitude drop of the residuals” is not sufficient to avoid contamination of the solution with iterative errors;

- The assessment of the statistical convergence levels shows that SRS models are substantially more demanding than RANS. Moreover, for \overline{C}_D the available simulation time is not enough to converge the statistics of this quantity;
- Naturally, the influence of the time-step on the numerical uncertainty is stronger for the SRS models than for the RANS models due to the nature of the dependent variables of the models;
- Logically, the explicit dependence of the SRS models on the grid size makes them more sensitive to grid refinement than RANS. However, the most important trend found in this study is that attaining negligible levels of numerical uncertainty, when compared to modelling errors, requires much finer grids than what is typically found in the open literature;
- Overall, the results suggest that the selected hybrid mathematical models are able to reduce the modelling error when compared to RANS. As expected, hybrid models are more expensive than RANS models, but the increase in cost is justified by an improvement in the modelling accuracy. However, a reliable assessment of such models is a challenging task due to the resources required to attain negligible numerical uncertainties.

In future we will perform a similar exercise for a higher Reynolds number case: the flow past a circular cylinder at $Re = 1.4 \times 10^5$. Moreover, we will test two additional hybrid models: the SAS and Partially-Averaged Navier-Stokes (PANS) equations.

REFERENCES

- [1] Menter, F.R., Kuntz, M., Bender, R. A Scale-Adaptive Simulation Model for turbulent Flow Predictions. *In Proceedings of the 41st American Institute of Aeronautics and Astronautics Aerospace Science Meeting and Exhibit*, 2003, January 6-9, Reno, United States of America.
- [2] Spalart, P.R., Jou, W-H., Strelets, M., Allmaras, S.R. Comments on the Feasibility of LES for Wings, and on a Hybrid RANS/LES Approach. *In Proceedings of the 1st Air Force Office of Scientific Research International Conference on DNS/LES*, 1997, August 4-8, Ruston, United States of America.
- [3] Kok, J.C., Dol, H.S., Oskam, B., van der Van, H. Extra-Large Eddy Simulation of Massively Separated Flows. *In Proceedings of the 42nd American Institute of Aeronautics and Astronautics Aerospace Sciences Meeting and Exhibit*, 2004, January 5-8, Reno, United States of America.
- [4] ReFRESH, 2015. <http://www.refresco.org>

- [5] Menter, F.R., Kuntz, M., Langtry, R. Ten Years of Industrial Experience with the SST Turbulence Model. *In Proceedings of the Turbulence, Heat and Mass Transfer IV*, 2003, October 12-17, Antalya, Turkey.
- [6] Gritskevich, M.S., Garbaruk, A.V., Schütze, J., Menter, F.R. Development of DDES and IDDES Formulations for the $k - \omega$ Shear Stress Transport Model. *Flow, Turbulence and Combustion*, 2012, **88**(3):431-449.
- [7] Kok, J.C. Resolving the Dependence on Freestream Value for the $k - \omega$ Turbulence Model. *American Institute of Aeronautics and Astronautics Journal*, 2000, **38**(7):1292-1295.
- [8] Pereira, F.S., Vaz, V., Eça, L. Flow Past a Circular Cylinder: A Comparison Between RANS and Hybrid Turbulence Models for a Low Reynolds Number. *In Proceedings of the 34th International Conference on Ocean, Offshore and Arctic Engineering*, 2015, May 31 - June 5, St. John's, Canada.
- [9] Eça, L., Hoekstra, M. A Procedure for the Estimation of the Numerical Uncertainty of CFD Calculations Based on Grid Refinement Studies. *Journal of Computational Fluids*, 2014, **262**:104-130.
- [10] Brouwer, J., Tukker, J., van Rijsbergen, M. Uncertainty Analysis of Finite Length Measurement Signals. *In Proceedings of the 3rd International Conference on Advanced Model Measurement Technology for EU Maritime Industry*, 2013, September 17-18, Gdansk, Poland.
- [11] Brouwer, J. (private communication).
- [12] Norberg, C. Effects of Reynolds Number and a Low-Intensity Freestream Turbulence on the Flow Around a Circular Cylinder. *Publikation 87/2*, 1987, Chalmers University of Technology.
- [13] Norberg, C. Flow Around a Circular Cylinder: Aspects of Fluctuating Lift. *Journal of Fluids and Structures*, 2001, **15**(3-4):459-469.
- [14] Parnaudeau, P., Carlier, J., Heitz, D., Lamballais, E. Experimental and Numerical Studies of the Flow Over a Circular Cylinder at Reynolds Number 3900. *Physics of Fluids*, 2008, **20**:085101.